

Ab Initio Description of Disordered $\text{Sr}_{1-x}\text{K}_x\text{Fe}_2\text{As}_2$ Using the Coherent Potential Approximation

Jiji J. Pulikkotil and Udo Schwingenschlöggl*

KAUST, PSE Division, Thuwal 23955-6900, Saudi Arabia

(Received 13 March 2010; published 29 April 2010)

The electronic structure of disordered $\text{Sr}_{1-x}\text{K}_x\text{Fe}_2\text{As}_2$ is studied by *ab initio* density functional theory. As no superstructure and/or atomic short range ordering is reported for $\text{Sr}_{1-x}\text{K}_x\text{Fe}_2\text{As}_2$, the coherent potential approximation can be used to describe the effects of chemical disorder. We find clear deviations from the rigid band model characteristics. Nonmagnetic calculations show an enhancement of the density of states at the Fermi energy in the range $0.4 \leq x \leq 0.65$, which coincides with the region where experiments observe an enhanced superconducting transition temperature, and antiferromagnetic calculations indicate a significant renormalization of states at Fermi energy. Analyzing the distribution of the Fe $3d$ states over the range $0 \leq x \leq 1$ we propose an effective three band model.

DOI: 10.1103/PhysRevLett.104.177006

PACS numbers: 74.70.Xa

The emergence of superconductivity in the recently discovered $A\text{Fe}_2\text{As}_2$ ($A = \text{Ca}, \text{Sr}, \text{Ba}, \text{and Eu}$) [1,2] compounds seems to be associated with the suppression of magnetic ordering, which is accomplished either via application of pressure [2–4] or by chemical substitutions [1,5–9]. Under ambient conditions, the materials are antiferromagnetic (AFM) with stripelike alignment of the Fe local moments in the basal plane of the tetragonal unit cell. The superconducting transition temperature (T_C) is enhanced up to ~ 25 K via electron doping in the Fe-As layers [6–10]. However, much higher values of T_C are achieved via hole doping in the A sublattice. For example, superconductivity in $\text{Sr}_{1-x}\text{K}_x\text{Fe}_2\text{As}_2$ emerges at $x = 0.17$ and peaks to 37 K at $x = 0.45$ [11]. In the narrow range $0.15 \leq x \leq 0.30$ the magnetic and superconducting transitions appear as successive transitions upon cooling [12,13]. For $x > 0.45$, T_C decreases and eventually saturates at ~ 3 K when x approaches a value of 1.0.

The onset of superconductivity and the disappearance of long range magnetic ordering seems to be intimately related to the changes in the Fermi surface. Two distinct features, namely, the hole pockets around the Brillouin-zone center (Γ point) and electron pockets at the zone corners (M point) are deduced for the undoped materials. Spectroscopic measurements show significant renormalization of these surfaces as a function of hole doping [14–17]. It is observed that with increasing hole concentration the hole pockets remain more or less unaltered, while the electron pockets gradually disappear as x increases from $x = 0$ to $x = 1$ in $A_{1-x}\text{K}_x\text{Fe}_2\text{As}_2$ [15]. However, it is interesting to note that the disappearance of the electron pockets does not corroborate with T_C . In fact, the highest T_C is obtained for a chemical composition of $x \approx 0.5$ in the phase diagram, whereas further increase in the K concentration leads to the suppression of superconductivity.

From the theoretical frontier, effects of doping on the electronic structure of $A\text{Fe}_2\text{As}_2$ materials, have been

studied by first-principles calculations. Because of its high electropositive nature the A ion in $A\text{Fe}_2\text{As}_2$ is fully ionized and therefore does not show any significant contribution to the valence band. Thus, on a first glance, it may be expected that doping with K, which introduces holes, would merely lower the Fermi energy (E_F) and that the rigid band model (RBM) would hold for these materials. If the latter model holds, one expects an increase in the density of states at the Fermi energy $D(E_F)$. Both the virtual crystal approximation (VCA) [18] and supercell calculations [19] have been used to study the effects of disorder in $A\text{Fe}_2\text{As}_2$ materials. While supercell calculations for doped compounds find a significant increase in $D(E_F)$, VCA studies find that $D(E_F)$ remains rather insensitive to the hole doping concentration. It is interesting to note that the VCA, which may be considered as the most sophisticated model to describe RBM characteristics, in fact deviates from the RBM predictions itself. According to Stern [20], the RBM could be considered as an appropriate model if the valencies of the impurity and the host atom are similar. In this context, the validity of the RBM for Co/Ni substitutions in the Fe sublattice, as reported earlier [21], seems to work well since Fe, Co, and Ni have a formal valence of +2 in the $A\text{Fe}_2\text{As}_2$ compounds.

The modern *ab initio* theory of electronic structure of substitutionally disordered materials [22,23] is based on the coherent potential approximation (CPA) [24]. In this formalism, a random array of real muffin-tin potential wells is replaced by effective wells. The scattering properties of this effective potential are then determined self-consistently from the requirement that an electron traveling in an infinite array of effective wells undergoes, on average, no further scattering upon replacement of a single effective potential with a real muffin-tin potential well. The method has been successfully used to study the physical properties of a variety of disordered materials and is argued to be a clear improvement over the VCA and other RBM based model Hamiltonians [22].

In this Letter we analyze the changes in the electronic structure of $\text{Sr}_{1-x}\text{K}_x\text{Fe}_2\text{As}_2$ for the full range $0 \leq x \leq 1$.

The normal metal state properties are calculated using the Korringa-Kohn-Rostoker (KKR) method formulated in the atomic sphere approximation (ASA) [25]. The potential of the disordered material is modeled in the CPA. For improving the alloy energetics, the ASA is corrected by both the muffin-tin correction and the multipole moment correction to the Madelung potential and energy. These corrections significantly improve the accuracy of the total energy by taking into account the nonspherical part of the polarization effects [26,27]. The partial waves in the KKR-ASA calculations are expanded up to $l_{\text{max}} = 3$ inside the muffin-tin spheres although the multipole moments of the electron density are determined up to $l_{\text{max}} = 6$. The exchange correlation effects are taken into consideration via the local density approximation (LDA). The core states are recalculated after each iteration. The calculations are scalar relativistic in the sense that first order perturbation corrections to the energy eigenvalues due to the Darwin and mass-velocity terms are included. The atomic sphere radii for Sr(K), Fe, and As are 1.393, 0.851, and 0.810 Wigner-Seitz radii, respectively. The overlap volume resulting from the blowup of the atomic spheres is less than 17%, which is legitimate within the accuracy of the approximation. For the total energy convergence, 252 k points are used in the irreducible part of the Brillouin zone. Convergence of the charge density is achieved such that the root-mean square of moments of the occupied partial density of states (DOS) becomes smaller than 10^{-6} .

Experiments as well as theoretical calculations show that the ground state magnetic structure of SrFe_2As_2 is antiferromagnetic with stripelike arrangement of the Fe local moments [28,29]. However, there are inconsistencies regarding the magnitude of the local moments. While experiments find a Fe local moment in SrFe_2As_2 of $\sim 1.0\mu_B$ [30], theoretical calculations find moments of 1.6–0.9 μ_B [29,31]. The variation in the calculated Fe magnetic moments in the theoretical calculations is due to the position of the As ion, which is not fixed by crystal symmetry. Relaxation of the As position by first-principles methods shows a significant deviation from the experimental value. The exact value of the As(z) coordinate is also found to be sensitive to the choice of the exchange correlation potential used in the crystal Hamiltonian. Calculations with the experimental value of the As(z) parameter, however, find large Fe local magnetic moments. A result closer to experiment is obtained for the theoretically optimized value of As(z) = 0.352.

In Fig. 1 we show the nonmagnetic total DOS of $\text{Sr}_{1-x}\text{K}_x\text{Fe}_2\text{As}_2$. The overall features of the spectra for $x = 0$ are in good agreement with previous results [32]. The upper valence band and the lower conduction band of the spectra are dominated by the Fe 3d states. Although small, the As 4p states are widespread in energy, suggesting strong covalent hybridization with the Fe 3d states. For SrFe_2As_2 , the Fermi energy is bounded by a Fe 3d derived

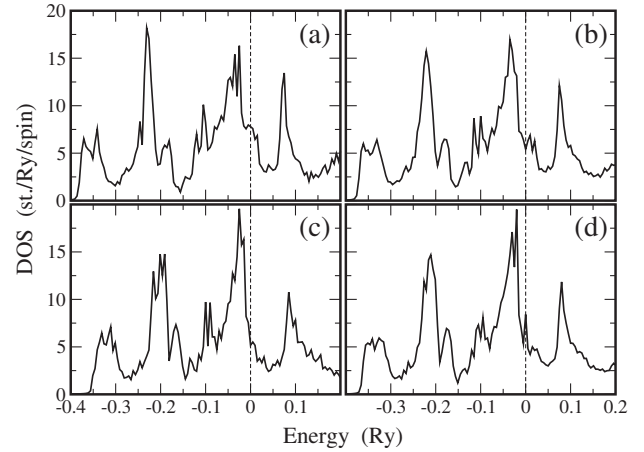


FIG. 1. Nonmagnetic total DOS of $\text{Sr}_{1-x}\text{K}_x\text{Fe}_2\text{As}_2$ for (a) $x = 0.0$, (b) $x = 0.40$, (c) $x = 0.65$, and (d) $x = 1.0$. The vertical line at the energy zero in each panel correspond to the relative Fermi energy.

peak around -45 mRy and by a pseudogap around $+35$ mRy. The pseudogap, in fact, manifests the separation of the bonding from the antibonding states. With increasing x in $\text{Sr}_{1-x}\text{K}_x\text{Fe}_2\text{As}_2$ the electron count decreases and E_F is lowered. Similar to the undoped case, we find that for the entire composition range $0 \leq x \leq 1$, the predominant features in the DOS are largely constituted by the Fe 3d states. Analysis shows that the center of the Fe 3d bands is shifted by 6 mRy towards E_F as x increases from $x = 0$ to $x = 1$. The bottom of the upper valence band also is shifted by 20 mRy towards E_F for KFe_2As_2 as compared to SrFe_2As_2 . Both these features illustrate that there is a progressive localization of the Fe 3d states when the K concentration increases in $\text{Sr}_{1-x}\text{K}_x\text{Fe}_2\text{As}_2$. Beyond, we find that, due to the decreasing electron count, E_F of the disordered material comes closer to the Fe 3d resonance peak. For KFe_2As_2 , this peak is located 15 mRy below E_F , indicating a significant shift of 30 mRy in comparison to SrFe_2As_2 .

The changes in the DOS spectra of $\text{Sr}_{1-x}\text{K}_x\text{Fe}_2\text{As}_2$ as a function of hole doping clearly show the invalidity of the RBM in these disordered materials. One finds a significant modification of the states at E_F . The Fermi energy, which is placed on a plateaulike feature for SrFe_2As_2 , is altered upon disorder, showing a gradual evolution of a new peak at $x \sim 0.45$. To illustrate how $D(E_F)$ changes with x in $\text{Sr}_{1-x}\text{K}_x\text{Fe}_2\text{As}_2$ we refer to Fig. 2. The calculated $D(E_F)$ for SrFe_2As_2 is estimated to be 7.8 st./Ry/atom/spin, which is consistent with previous band structure data [32]. For small K concentrations, $D(E_F)$ initially decreases by a small amount and then increases steadily over the range $0.45 \leq x \leq 0.65$. The trend for a small K concentration is consistent with earlier VCA calculations [18], while the increase for $x = 0.5$ is consistent with earlier supercell data [19]. For $x > 0.65$ in $\text{Sr}_{1-x}\text{K}_x\text{Fe}_2\text{As}_2$, $D(E_F)$ decreases monotonically. Coincidentally, the highest T_C reported in the $\text{Sr}_{1-x}\text{K}_x\text{Fe}_2\text{As}_2$ phase diagram is in the

regime where our calculations find an increase in $D(E_F)$, i.e., in the range $0.40 \leq x \leq 0.65$. To further analyze the variation in the nonmagnetic $D(E_F)$ as a function of x we shown in Fig. 2 (lower panel) the Fe 3d orbital resolved $D(E_F)$. It appears that the changes in the variation of $D(E_F)$ upon K substitution are determined by the Fe d_{xz} and d_{xy} bands. The variation in the Fe $d_{x^2-y^2}$, d_{3z^2-1} and d_{yz} bands remains more or less constant across the composition range.

In Fig. 3, we show the changes in the spin polarized antiferromagnetic total DOS for $\text{Sr}_{1-x}\text{K}_x\text{Fe}_2\text{As}_2$. The corresponding variation in $D(E_F)$ (upper panel) and the Fe 3d orbital resolved DOS (lower panel) as a function of the K concentration are shown in Fig. 2. The DOS of SrFe_2As_2 is in good agreement with previous reports [33]. Similar to the nonmagnetic counterpart, the top of the valence band and the lower conduction band are mostly composed of the Fe 3d states. For SrFe_2As_2 , E_F is positioned in a pseudogap bounded by two peaks located at -35 and $+10$ mRy. Detailed analysis of these two peaks in terms of the orbital resolved DOS shows that the peak below E_F is predominantly composed of the Fe d_{3z^2-1} , d_{xy} , and d_{xz} states, while the peak just above E_F is composed of the Fe d_{xz} , d_{yz} , and d_{xy} states. We note that a strong correspondence has been emphasized between the pseudogap and structural stability, since the pseudogap refers to a complete filling of the bonding states. Beyond, our analysis shows that the pseudogap is mainly composed of the Fe d_{xy} states, with a contribution twice larger than that of the d_{3z^2-1} , d_{xz} , d_{yz} , and $d_{x^2-y^2}$ states. The latter four states appear to be more or

less uniformly composed; see Fig. 2 for $x = 0$. For SrFe_2As_2 , $D(E_F)$ is calculated to be 2.5 st./Ry/spin.

With increasing K concentration in $\text{Sr}_{1-x}\text{K}_x\text{Fe}_2\text{As}_2$ the overall shape of the AFM DOS barely changes. It is interesting to note that the sharp structures in the upper valence band are little modified upon increasing disorder. The decreasing electron count with increasing K concentration, leads to a lowering of E_F . Furthermore, the variation in $D(E_F)$ deviates from the predictions of the RBM, much like in the nonmagnetic case, as described above. Over the range $0.0 \leq x \leq 0.4$, we find little or no change in the variation of $D(E_F)$. However, for $x > 0.45$, $D(E_F)$ increases steadily. For KFe_2As_2 , $D(E_F)$ is determined to be 3.6 st./Ry/spin. One may also note that the pseudogap becomes narrower and accommodates fewer states with decreasing electron count. The progressive shift of E_F towards the bonding region, which is in the lower energy regime, and the corresponding changes in the pseudogap suggest a significant renormalization of states at E_F with increasing K concentration.

Turning to magnetism, we analyze the exchange splitting of the local Fe 3d bands in $\text{Sr}_{1-x}\text{K}_x\text{Fe}_2\text{As}_2$. For SrFe_2As_2 , the centers of the majority and minority Fe 3d bands are estimated to be at -95 and -12 mRy. These values progressively shift towards E_F as the K concentration increases. For KFe_2As_2 , the positions of the Fe 3d majority and minority band centers are estimated to be -75 and -2 mRy. These values yield a local exchange Fe 3d band splitting of 83 and 73 mRy for SrFe_2As_2 and KFe_2As_2 , respectively. For a given Stoner parameter I , the exchange band splitting is proportional to the magnitude of the local magnetic moment. In this regard, one would expect a finite sizable moment for Fe in $\text{Sr}_{1-x}\text{K}_x\text{Fe}_2\text{As}_2$ compounds. The magnetic moments of SrFe_2As_2 and KFe_2As_2 are 1.2 and $1.1 \mu_B$, respectively, and for intermediate compositions the variation is deter-

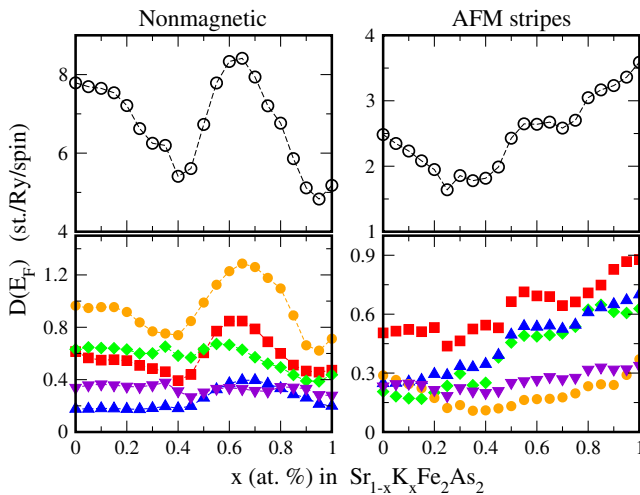


FIG. 2 (color online). Upper panel: Variation of the density of states at the Fermi energy, $D(E_F)$. Lower panel: Fe 3d orbital decomposed contributions of $\text{Sr}_{1-x}\text{K}_x\text{Fe}_2\text{As}_2$ for nonmagnetic and AFM stripes over the range $0 \leq x \leq 1$ in $\text{Sr}_{1-x}\text{K}_x\text{Fe}_2\text{As}_2$. In the lower panels, the symbols with circles (orange), squares (red), diamonds (green), triangles up (blue), and triangles down (violet) represent the Fe d_{xz} , d_{xy} , d_{yz} , d_{3z^2-1} , and $d_{x^2-y^2}$ states, respectively.

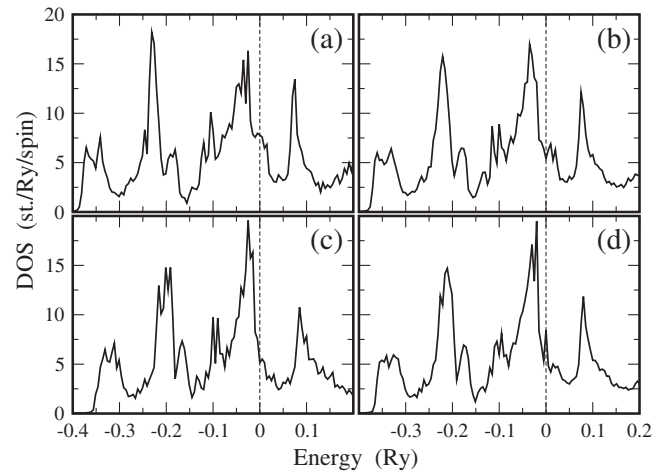


FIG. 3. Antiferromagnetic total DOS of $\text{Sr}_{1-x}\text{K}_x\text{Fe}_2\text{As}_2$ for (a) $x = 0.0$, (b) $x = 0.40$, (c) $x = 0.65$, and (d) $x = 1.0$. The vertical line at the energy zero in each panel corresponds to the relative Fermi energy.

mined to be linear. In fact, we note that the magnitude of the moment is sensitive to the exact position of the As atom with respect to the Fe sublattice. An earlier report estimates the magnetic moments in SrFe_2As_2 and KFe_2As_2 to be 1.69 and $1.58\mu_B$, respectively [29]. The discrepancy in the calculated magnitudes of the magnetic moments may be associated with the local geometry of the Fe-As layers, in which small variations in the As(z) coordinate lead to drastic changes in the magnetic properties. However, we note that the present Letter focuses on the role of electronic effects on the physical properties.

In conclusion, we have carried out first-principles calculations for $\text{Sr}_{1-x}\text{K}_x\text{Fe}_2\text{As}_2$ in the composition range $0 \leq x \leq 1$, based on the KKR-ASA-CPA method of electronic structure theory. Neglecting the effects of local geometry changes in the Fe-As layers upon increasing K concentration, our calculations show distinct deviations from the prediction of the RBM. In the nonmagnetic case, we obtain an enhanced $D(E_F)$ in the same range, $0.40 \leq x \leq 0.65$, in which experiments find an enhanced superconductivity. The AFM calculations point to a significant renormalization of the electronic states as compared to their nonmagnetic counterparts. Beyond, the analysis of the Fe orbital resolved DOS paves the way to an effective multiband model. For SrFe_2As_2 , one may approximate the AFM electronic structure by two effective bands given by the d_{xy} states and an amalgamation of the d_{3z^2-1} , d_{xz} , d_{yz} , and $d_{x^2-y^2}$ states. With increasing K concentration, the states split into three effective bands, namely, the d_{xz} , $d_{x^2-y^2} + d_{3z^2-1}$, and $d_{xy} + d_{yz}$ bands. This splitting shows up right when $x \sim 0.4$, i.e., where the highest T_C is observed in experiment.

*udo.schwingenschlogl@kaust.edu.sa

- [1] M. Rotter, M. Tegel, and D. Johrendt, *Phys. Rev. Lett.* **101**, 107006 (2008).
- [2] P.L. Alireza, Y.T.C. Ko, J. Gillett, C.M. Petrone, J.M. Cole, G.G. Lonzarich, and S.E. Sebastian, *J. Phys. Condens. Matter* **21**, 012208 (2009).
- [3] M.S. Torikachvili, S.L. Bud'ko, N. Ni, and P.C. Canfield, *Phys. Rev. Lett.* **101**, 057006 (2008).
- [4] T. Park, E. Park, H. Lee, T. Klimczuk, E.D. Bauer, F. Ronning, and J.D. Thompson, *J. Phys. Condens. Matter* **20**, 322204 (2008).
- [5] Y. Kamihara, T. Watanabe, M. Hirano, and H. Hosano, *J. Am. Chem. Soc.* **130**, 3296 (2008).
- [6] A.S. Sefat, R. Jin, M.A. McGuire, B.C. Sales, D.J. Singh, and D. Mandrus, *Phys. Rev. Lett.* **101**, 117004 (2008).
- [7] S. Jiang, H. Xing, G. Xuan, Z. Ren, C. Wang, Z.A. Xu, and G. Cao, *Phys. Rev. B* **80**, 184514 (2009).
- [8] N. Kumar, S. Chi, Y. Chen, K.G. Rana, A.K. Nigam, A. Thamizhavel, W. Ratcliff, S.K. Dhar, and J.W. Lynn, *Phys. Rev. B* **80**, 144524 (2009).
- [9] D.K. Pratt, W. Tian, A. Kreyssig, J.L. Zarestky, S. Nandi, N. Ni, S.L. Bud'ko, P.C. Canfield, A.I. Goldman, and R.J. McQueeney, *Phys. Rev. Lett.* **103**, 087001 (2009).
- [10] S.R. Saha, N.P. Butch, K. Kirshenbaum, and J. Paglione, *Phys. Rev. B* **79**, 224519 (2009).
- [11] K. Sasmal, B. Lv, B. Lorenz, A.M. Guloy, F. Chen, Y.Y. Xue, and C.W. Chu, *Phys. Rev. Lett.* **101**, 107007 (2008).
- [12] M. Gooch, B. Lv, B. Lorenz, A.M. Guloy, and C.W. Chu, *Phys. Rev. B* **78**, 180508(R) (2008).
- [13] B. Lv, M. Gooch, B. Lorenz, F. Chen, A.M. Guloy, and C.W. Chu, *New J. Phys.* **11**, 025013 (2009).
- [14] H. Liu, W. Zhang, L. Zhao, X. Jia, J. Meng, G. Liu, X. Dong, G.F. Chen, J.L. Luo, N.L. Wang, W. Lu, G. Wang, Y. Zhou, Y. Zhu, X. Wang, Z. Xu, C. Chen, and X.J. Zhou, *Phys. Rev. B* **78**, 184514 (2008).
- [15] T. Sato, K. Nakayama, Y. Sekiba, P. Richard, Y.-M. Xu, S. Souma, T. Takahashi, G.F. Chen, J.L. Luo, N.L. Wang, and H. Ding, *Phys. Rev. Lett.* **103**, 047002 (2009).
- [16] A. Koitzsch, D.S. Inosov, D.V. Evtushinsky, V.B. Zabolotnyy, A.A. Kordyuk, A. Kondrat, C. Hess, M. Knupfer, B. Büchner, G.L. Sun, V. Hinkov, C.T. Lin, A. Varykhalov, and S.V. Borisenko, *Phys. Rev. Lett.* **102**, 167001 (2009).
- [17] T. Kondo, R.M. Fernandes, R. Khasanov, C. Liu, A.D. Palczewski, N. Ni, M. Shi, A. Bostwick, E. Rotenberg, J. Schmalian, S.L. Bud'ko, P.C. Canfield, and A. Kaminski, *Phys. Rev. B* **81**, 060507(R) (2010).
- [18] D.J. Singh, *Phys. Rev. B* **78**, 094511 (2008).
- [19] I.R. Shein and A.L. Ivanovskii, arXiv:0807.0984.
- [20] E.A. Stern, *Phys. Rev.* **157**, 544 (1967).
- [21] A. Leithe-Jasper, W. Schnelle, C. Geibel, and H. Rosner, *Phys. Rev. Lett.* **101**, 207004 (2008).
- [22] J.S. Faulkner, *Prog. Mater. Sci.* **27**, 1 (1982).
- [23] J.S. Faulkner and G.M. Stocks, *Phys. Rev. B* **21**, 3222 (1980).
- [24] P. Soven, *Phys. Rev.* **178**, 1136 (1969).
- [25] A.V. Ruban and H.L. Skriver, *Comput. Mater. Sci.* **15**, 119 (1999).
- [26] A.V. Ruban and H.L. Skriver, *Phys. Rev. B* **66**, 024201 (2002).
- [27] A.V. Ruban, S.I. Simak, P.A. Korzhavyi, and H.L. Skriver, *Phys. Rev. B* **66**, 024202 (2002).
- [28] A. Jesche, N. Caroca-Canales, H. Rosner, H. Borrmann, A. Ormeci, D. Kasinathan, H.H. Klauss, H. Luetkens, R. Khasanov, A. Amato, A. Hoser, K. Kaneko, C. Krellner, and C. Geibel, *Phys. Rev. B* **78**, 180504(R) (2008).
- [29] M.J. Han, Q. Yin, W.E. Pickett, and S.Y. Savrasov, *Phys. Rev. Lett.* **102**, 107003 (2009).
- [30] J. Zhao, W. Ratcliff, J.W. Lynn, G.F. Chen, J.L. Luo, N.L. Wang, J. Hu, and P. Dai, *Phys. Rev. B* **78**, 140504(R) (2008).
- [31] Y. Lee, D. Vaknin, H. Li, W. Tian, J.L. Zarestky, N. Ni, S.L. Bud'ko, P.C. Canfield, R.J. McQueeney, and B.N. Harmon, *Phys. Rev. B* **81**, 060406(R) (2010).
- [32] D. Kasinathan, A. Ormeci, K. Koch, U. Burkhardt, W. Schnelle, A. Leithe-Jasper, and H. Rosner, *New J. Phys.* **11**, 025023 (2009).
- [33] I.R. Shein and A.L. Ivanovskii, *Physica (Amsterdam)* **469C**, 15 (2009).